NUMERICAL MODELLING OF MOORING SYSTEMS FOR FLOATING WAVE ENERGY CONVERTERS
Modelação Numérica de Sistemas de Amarração para Conversores Flutuantes de Energia das Ondas

GUILHERME MOURA PAREDES (1), JOHANNES PALM (2), CLAES ESKILSSON (3),
LARS BERGDAHL (4) and FRANCISCO TAVEIRA PINTO (5)

(1) Doctoral student, FEUP,
Rua Dr. Roberto Frias, s/n 4200-465 Porto, Portugal, moura.paredes@fe.up.pt
(2) Doctoral Student. Chalmers University of Technology,
Chalmers University of Technology, SE-412 96, johannes.palm@chalmers.se
(3) Researcher, Chalmers University of Technology,
Chalmers University of Technology, SE-412 96, claes.eskilsson@chalmers.se
(4) Professor Emeritus. Chalmers University of Technology,
Chalmers University of Technology, SE-412 96, lars.bergdahl@chalmers.se
(5) Full Professor, FEUP,
Rua Dr. Roberto Frias, s/n 4200-465 Porto, Portugal, fpinto@fe.up.pt

Abstract

A numerical model (MOODY) for the study of the dynamics of cables is presented in Palm *et al.* (2013), which was developed for the design of mooring systems for floating wave energy converters. But how does it behave when it is employed together with the tools used to model floating bodies? To answer this question, MOODY was coupled to a linear potential theory code and to a computational fluid dynamics code (OpenFOAM), to model small scale experiments with a moored buoy in linear waves. The experiments are well reproduced in the simulations, with the exception of second order effects when linear potential theory is used and of the small overestimation of the surge drift when computational fluid dynamics is used. The results suggest that MOODY can be used to successfully model moored floating wave energy converters.

Keywords: Mooring, wave energy converter, hp-finite element, numerical simulation, cable.

Resumo

Palm *et al.* (2013) apresentam um modelo numérico (MOODY) desenvolvido para o estudo da dinâmica de cabos de amarrações de conversores flutuantes de energia das ondas. Mas como é que se comporta o modelo quando é aplicado em conjunto com as ferramentas utilizadas para simular corpos flutuantes? Para responder a esta questão, foi feito o acoplamento do MOODY a um código de teoria potencial linear e a um código de mecânica dos fluidos computacional (OpenFOAM) para recriar experiências em modelo reduzido com uma bóia amarrada sujeita a ondas lineares. As experiências são bem reproduzidas nas simulações, à excepção dos efeitos de segunda ordem quando é utilizada a teoria potencial linear e uma ligeira sobrestimação da deriva quando é utilizada mecânica dos fluidos computacional. Os resultados indicam que o MOODY pode ser utilizado para modelar com sucesso o sistema de amarração de conversores flutuantes de energia das ondas.

Palavras-chave: Amarração, conversor de energia das ondas, elemento finito hp, simulação numérica, cabo.

1. Introduction

With the objective of providing tools to study mooring systems for wave energy converters, a numerical model for the dynamics of cables, MOODY (Palm *et al.*, 2013) was developed. MOODY extends the higher-order finite element formulation of (Montano *et al.*, 2007) by allowing the tension to vary within each element and by using a fully discontinuous formulation, the Local Discontinuous Galerkin formulation (LDG) (Cockburn and Shu, 2001).

It was needed to know how would MOODY perform when applied to realistic situations together with the usual "tools of the trade" for simulation of moored floating bodies.

For this reason, two approaches to simulate floating bodies were selected: the simple, industry standard, linear potential theory and the high-end, intensive, computational fluid dynamics (CFD).

An in-house code was used for simulations with linear potential theory and the open source package OpenFOAM was used for simulations with computational fluid dynamics. MOODY is coupled to each of the codes to enable a complete simulation of a moored buoy floating in water.

Linear potential theory is a fast and reliable approach for small amplitude motions, but lacks second order effects that may be important.

Computational fluid dynamics is computationally intensive, but provides the opportunity to study non-linear phenomena, where linear potential theory breaks down.

The simulations recreated small scale laboratory experiments with linear waves. This wave regime is similar to the one where wave energy devices are expected to operate. The behaviour of MOODY under "operating conditions" for wave energy converters can, therefore, be assessed.

In this study it is assumed that the cables do not have bending stiffness, which may be important when the tension is low.

The results show that MOODY can be used in the study of moored structures. The motions and tensions measured in the laboratory experiments are reasonably well reproduced using the numerical model. There are limitations caused by the fact that linear potential theory doesn't account for second order drift forces (underestimating surge motions) and by the large fluctuations in the air phase in the CFD simulations (overestimating surge motions).

A deeper coverage of the small scale experiments and the simulations using linear potential theory can be found in Paredes *et al.* (2013) and of those using computational fluid dynamics in Palm *et al.* (2013).

2. Governing Equations of Moored Bodies

2.1. Flexible cable dynamics

The dynamics of cables are simulated using the equation of flexible cables, in a non-dimensional form as presented in Lindahl (1985),

$$\frac{\partial^2 \mathbf{r}}{\partial t^2} = \frac{\partial}{\partial s}\left(\frac{1}{m_l}\frac{t_c^2}{L_c^2}\frac{T}{(1+\epsilon)}\frac{\partial \mathbf{r}}{\partial s}\right) + \mathbf{f} \qquad [1]$$

where t is the non-dimensional time, $\mathbf{r}$ is the non-dimensional position vector, S is the non-dimensional curvilinear abscissa along the cable (unstretched), m_l is the mass per unit length of the cable (unstretched), T is the tension, ϵ is the strain, $\mathbf{f}$ is the non-dimensional vector of the external forces acting on the cable, L_C is a characteristic length and t_c is a characteristic time. The characteristic length L_C is chosen to be the length of the cable and the characteristic time t_c is the time it takes for a shock wave to propagate along the cable. The celerity of a shock wave C, for a thin cable is given by

$$c = \sqrt{\frac{K}{m_l}} \qquad [2]$$

where K is the stiffness of the cable.

The position vector $\mathbf{r}$ and the abscissa along the cable S are made non-dimensional by scaling them with L_c and the time t is made non-dimensional by scaling it with t_c.

The tension in the cable is determined using Hooke's law, Eq. [3] where the extension is computed using the following definition

$$T = K\epsilon \qquad [3]$$

$$\epsilon = \left\|\frac{\partial \mathbf{r}}{\partial s}\right\| - 1 \qquad [4]$$

To solve Eq.[1], MOODY uses *hp*-finite elements with a modified version of the Local Discontinue Galerkin formulation. MOODY is described in detail in Palm *et al.* (2013) and for brevity won't be described here.

The external forces acting on a submerged cable are the buoyancy, the weight, the hydrodynamic forces and the ground interaction forces.

The weight, the buoyancy and the hydrodynamic forces are modelled following the non-dimensionalizations presented in Lindahl (1985): the weight and the buoyancy are taken together as the submerged weight, Eq. [5], and the hydrodynamic forces are split into the inertia force, Eq. [6], the tangential drag force, Eq. [7] and the normal drag force, Eq. [8], using Morison's formula,

$$\mathbf{f}_b = \left(\frac{\rho_c - \rho_w}{\rho_c}\right)\frac{t_c^2}{L_c}\mathbf{g} \qquad [5]$$

$$\mathbf{f}_m = C_m \frac{A\rho_w}{m_l}\left(\mathbf{a}_{rel} - (\mathbf{a}_{rel}\cdot\mathbf{t})\mathbf{t}\right)(1+\epsilon) \qquad [6]$$

$$\mathbf{f}_{dt} = \frac{1}{2}C_{dt}\frac{\rho_w d L_c}{m_l}(\mathbf{v}_{rel}\cdot\mathbf{t})^2\,\mathbf{t}(1+\epsilon) \qquad [7]$$

$$\mathbf{f}_{dn} = \frac{1}{2}C_{dn}\frac{\rho_w d L_c}{m_l}\left|\left(\mathbf{v}_{rel} - (\mathbf{v}_{rel}\cdot\mathbf{t})\mathbf{t}\right)\right|\left(\mathbf{v}_{rel} - (\mathbf{v}_{rel}\cdot\mathbf{t})\mathbf{t}\right)(1+\epsilon) \qquad [8]$$

where ρ_w is the mass density of the fluid, ρ_c is the mass density of the cable, $\mathbf{f}_b$ is the submerged weight of the cable, $A$is the cross sectional area of the cable, $\mathbf{g}$ is the acceleration of gravity, $\mathbf{f}_m$and C_m are the added mass force and added mass coefficient, $\mathbf{f}_{dt}$ and C_{dt} are the tangential drag force and the tangential drag coefficient, $\mathbf{f}_{dn}$ and C_{dn} are the normal drag force and the normal drag coefficient, $\mathbf{v}_{rel}$ and $\mathbf{a}_{rel}$ are, respectively, the relative non-dimensional velocity and non-dimensional acceleration between the cable and the water, Eqs. [9] and [10], d is the nominal diameter of the cable and $\mathbf{t}$ is the tangential vector to the cable, Eq. [11].

$$\mathbf{v}_{rel} = \mathbf{v}_w - \frac{\partial \mathbf{r}}{\partial t} \qquad [9]$$

$$\mathbf{a}_{rel} = \mathbf{a}_w - \frac{\partial^2 \mathbf{r}}{\partial t^2} \qquad [10]$$

$$\mathbf{t} = \frac{\partial \mathbf{r}}{\partial s} / \left\|\frac{\partial \mathbf{r}}{\partial s}\right\| = \frac{\partial \mathbf{r}}{\partial s} / (1+\epsilon) \qquad [11]$$

where $\mathbf{v}_w$ and $\mathbf{a}_w$ represent the non-dimensional water velocity and acceleration.

The ground is modelled as a bi-linear spring-damper material in the normal direction and as surface with Coulomb friction in the tangential direction. In the normal direction, when the cable is settling on the ground, both stiffness and damping forces on the cable; when the cable is lifting, only the stiffness force is applied. This formulation prevents bouncing while allowing free lifting. In the horizontal direction, the ground applies a Coulomb friction force that is ramped from zero to its maximum value when the tangential velocity reaches a specified value.

2.2. Floating body dynamics

2.2.1. *Linear Potential Theory*

In the first simulation, the dynamics of the floating body are computed using linear potential theory. This approach models a floating body in waves as a spring-mass-damper system,

$$(\mathbf{M}+\mathbf{A})\ddot{\mathbf{x}}+\mathbf{B}\dot{\mathbf{x}}+\mathbf{C}\mathbf{x}=\mathbf{F} \qquad [12]$$

where $\mathbf{M}$ is the generalised mass matrix, $\mathbf{A}$ is the added inertia matrix, $\mathbf{B}$ is the radiation damping matrix, $\mathbf{C}$ is the hydrostatic stiffness matrix, $\ddot{\mathbf{x}}$, $\dot{\mathbf{x}}$ and $\mathbf{x}$ are, respectively, the acceleration, velocity and position vectors in the six degrees of freedom and $\mathbf{F}$ is the vector sum of all external forces and moments acting on the body, including wave induced forces, mooring forces, viscous drag and power take-off. The buoy dynamics are solved in their dimensional form.

Wave induced forces and moments are also computed following the linear potential theory formulations, given by

$$\mathbf{f}_{\mathrm{s}}=\mathbf{z}\eta\sin\left(\frac{2\pi}{T}t+\boldsymbol{\delta}\right) \qquad [13]$$

where $\mathbf{f}_{\mathrm{s}}$ is the vector of wave induced forces and moments, $\mathbf{z}$ is the vector of the wave force coefficients, η is the water surface elevation at the mean position of the floating body, T is the wave period, t is the time instant and $\boldsymbol{\delta}$ is the vector of the phase delay of the forces and moments relative to the phase of the wave. Eq. [12] is time-stepped via a leapfrog scheme.

2.2.2. *Computational Fluid Dynamics*

In the CFD simulations, the Euler equations, Eq.[14], are solved in the fluid domain (water and air) around the buoy,

$$\begin{aligned} &\nabla\cdot u=0 \\ &\frac{\partial u}{\partial t}+\nabla\left(\rho\left(u-u_{\mathrm{g}}\right)u\right)=-\nabla p+\rho f_{\mathrm{b}} \end{aligned} \qquad [14]$$

where u is the velocity of the fluid, u_{g} is the velocity grid used to discretise the fluid domain, p is the pressure and f_{b} is an external volume force.

The water pressure is integrated over the wetted surface of the hull of the buoy, to obtain the forces and moments around the centre of gravity. This takes into account all forces from transient effects such as overtopping green water or breaking waves.

To capture the free surface at the at the air-water interface, the Volume of Fluid method is used. This method computes the effective density ρ and the effective viscosity μ of a fluid as

$$\begin{aligned} \rho&=\alpha\,\rho_{\mathrm{w}}+(1-\alpha)\,\rho_{\mathrm{a}} \\ \mu&=\alpha\,\mu_{\mathrm{w}}+(1-\alpha)\,\mu_{\mathrm{a}} \end{aligned} \qquad [15]$$

where α is the volume fraction of water in the discretization element, ρ_{a} is the air density, μ_{a} is the air viscosity and μ_w is the water viscosity. For wave generation and absorption the *waves2Foam* package is used (Jacobsen *et al.*, 2012). Separate relaxation zones are used for the inlet and the outlet conditions.

2.3. Coupling

MOODY is a stand-alone code, but it has an interface that allows it to send and receive data to and from other codes. In the simulations presented in this work, the floating body solver gets the tension force on the cables from MOODY and computes the dynamics of the buoy. It then sends the new position of the attachment points of the cable to MOODY which, in turn, computes the evolution of the cable tension between the previous and the current position of the attachment. The tension force can, therefore, be expressed as the following function,

$$\mathbf{f}_{\mathrm{mo}}^{n}=f\left(t^{n},t^{n-1},\mathbf{p}^{n},\mathbf{p}^{n-1},\mathbf{r}^{n-1},\dot{\mathbf{r}}^{n-1},\dot{\mathbf{r}}^{n-1}\right) \qquad [16]$$

in which $\mathbf{f}_{\mathrm{mo}}^{\mathrm{n}}$ is the mooring force applied on the floating body, $\mathbf{p}^n$ and $\mathbf{p}^{n-1}$are the positions of the attachment point at the current, t^n, and previous, t^{n-1}, time step, and $\mathbf{r}^{n-1}$, $\dot{\mathbf{r}}^{n-1}$, and $\ddot{\mathbf{r}}^{n-1}$, are, respectively, the position, velocity and acceleration of the cable at the previous time step. The time steps required by MOODY and by the floating body solver aren't necessarily the same. If the time-step in MOODY is smaller than that of the floating body solver, MOODY interpolates the position of the attachment point between the previous and the current position.

3. Numerical Simulations of Moored WECs

3.1. Case description

The simulations presented here aim to recreate small scale experiments in a wave tank. The experimental setup is shown in Figure 1.

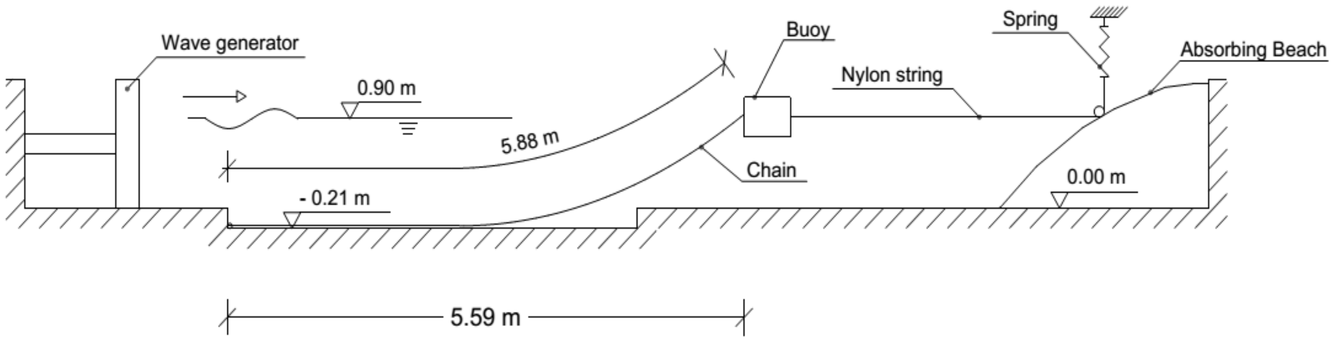

Figure 1. Experimental arrangement modelled in the numerical simulations. A cylindrical buoy moored by a catenary chain on the seaward side and by a nylon string connected to a linear spring on the leeward side. The moorings are parallel to the wave direction, which allows the setup to be reduced to a 2-dimensional problem.

The buoy was a vertical cylinder, with a mass of 35.28±0.05 kg and an inertia around the centre of floatation of 0.852±0.165 kg·m² In Figure 2 are represented the dimensions of the buoy, the position of the attachment points of the cables and the locations of the centre of gravity and of the centre of buoyancy. The position of centre of mass and the inertia were determined following the method described in Chakrabarti (1994).

Waves were generated travelling in a direction parallel to the plane of the mooring system. In this situation, the setup can be reduced to a 2-dimensional problem with three degrees of freedom: surge, heave and pitch.

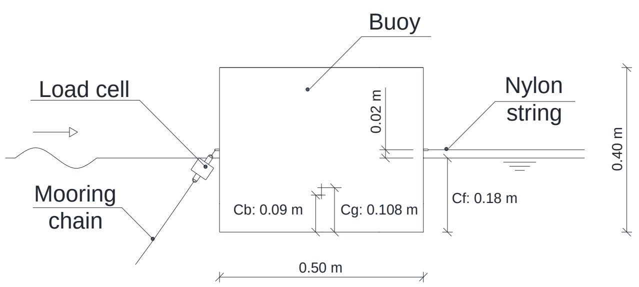

Figure 2. Detailed geometry of the buoy used in the experimental tests and modelled in the numerical simulations. Cb marks the position of the centre of buoyancy and Cg marks the position of the centre of gravity. Also represented is the placement of the load cell used to measure the tension in the seaward chain catenary and the position of the attachments of the mooring cables to the buoy.

The chain links were 16.6 mm long, 7.1 mm wide and 17mm thick. The dry weight per unit length of the chain was 0.436 N/m and its submerged weight per unit length was 0.382 N/m.

The spring was installed at the absorbing beach of the tank in the vertical position, so that its weight wouldn't interfere in the shape and tension of the nylon string.

The stiffness of the spring was 5.36 N/m. In the rest position of the buoy, the elongation of the spring was 0.243 m (subtracted the elongation caused by the weight of the spring), yielding a pre-tension of 1.3 N.

The nylon string had a negligible mass. It passed under a pulley so that it could be attached vertically to the spring, Figure 1.

In experimental tests, it was recorded the rigid body motions of the buoy, the tension at the fairlead end of the chain using an in-line submersible load cell, Figure 2, and the instantaneous water surface level at a point 2 m to the side of the rest position of buoy. This data was compared with the results of the simulations.

For brevity, out of all the conditions tested, the results for a regular wave of period $T = 1.4$ s and height $h = 0.100$ m are shown as an example in this article.

3.2. Mooring simulations

The chain was discretised using 10 elements, with 4^{th} degree polynomials of the Legendre type, yielding a total number of degrees of freedom of 60. The time step used in the cable simulation was 2×10^{-5} s.

Since chains cannot be compressed, a bilinear stress-strain relation for the chain was used, allowing tension, but not allowing compression.

The stiffness, the mass coefficient and the drag coefficients of the chain are presented in Table 1. These coefficients were taken from Lindahl (1985), where a set of experiments using a chain with dimensions similar to those used in this work it is described.

Table 1. Parameters used to model the chain (Lindahl, 1985): K – stiffness; C_{dt} – Tangential drag coefficient; C_{dn} – Normal drag coefficient; C_m – Added mass coefficient.

PARAMETER	VALUE
K	10 000 N/m
C_{dt}	0.5
C_{dn}	2.5
C_m	0.4129

For the non-dimensionalisation, the characteristic length L_C was the length of the chain (5.88 m) and the characteristic time was 0.0123 s. I

n the computation of the hydrodynamic forces acting on the chain, the nominal diameter used for the chain was 0.0027 m, determined as the diameter of a uniform cable of the same material as the chain (steel, with $\rho_{st} = 7800$ kg/m³), which would have the same mass per unit length.

The simulations using this discretisation are considered to be grid independent as the differences in the computed results using 5^{th} and 6^{th} degree polynomials with varying number of elements were negligible.

Like the chain, because the spring-string leg cannot go into compression, it was modelled as a bilinear material: it can stretch infinitely in the seaward direction, but will go slack for horizontal displacements larger than 0.243m in the leeward direction. Because the nylon string has a small mass and is almost horizontal when in tension (the angle to the horizontal is less than two degrees), the force applied by the nylon string on the buoy is assumed to be horizontal at all times.

Some simplifying assumptions had to be made when using linear potential theory.

As most of the chain catenary was hanging over the central pit (see Figure 1), in the simulation of the chain dynamics, the water depth used was 1.11 m. For the computation of the hydrodynamic forces acting on the chain, it is assumed that the water has neither velocity nor acceleration.

The added mass, radiation damping and wave exciting force coefficients for the linear simulations were determined using the formulation presented by Johansson (1986), for a cylinder oscillating in finite water depth. The coefficients are presented in Table 2.

In contrast to the assumptions of the formulations of Johansson (1986), where the bottom is assumed to be horizontal with a constant depth, there were two distinct water depths in the experimental setup.

Since the water depth under the buoy was 0.9 m, this was the value used in the computation of the coefficients, Table 2. The density of water was assumed to be $\rho_{\mathrm{w}} = 1000$ kg/m^3.

Table 2. Hydrodynamic coefficients of the cylindrical buoy. Aij – Added mass. Bij – Radiation damping. X_i – Excitation force coefficient. δ_i – phase delay. S – Surge. H – Heave. P – Pitch. SP – Couple surge-pitch.

	A_{ij}	B_{ij}	X_i	δ_i (rad)
S	23.92 kg	20.82 kg/s	963.8 N/m	1.501
H	27.05 kg	38.09 kg/s	921.8 N/m	0.206
P	0.2581kg.m²	0.01974 kg.m²/s	29.68 N	−1.641
SP	1.137 kg.m	0.6410 kg.m/s	-	-

The time step used for the buoy dynamics was 1×10^{-2}s in both codes; however, *OpenFOAM* has an automated time step size based on the Courant number which in practice decreased the time step to around 1×10^{-4}s.

4. Results

4.1. Linear Potential Theory

In Figure 3 are presented the tension at the attachment point of the chain and the motions of the centre of floatation of the buoy in the experiments and in the numerical simulations, for a regular wave with period $T = 1.4$ s and height $H = 0.100$ m.

The heave and pitch motions are correctly modelled, since both the amplitude and the mean oscillating position agree with the measurements.

The surge amplitude is well determined, but the mean surge position is underestimated (in the simulations it is close to the static position of the buoy while in the experiments the buoy is displaced by about 0.0275 m).

The tension is well captured, meaning that the maximum value and the general shape of the wave cycle are reproduced in the simulations. Details such as the small indentation in tension at the end of the rising leg are reproduced in the numerical simulations. After the peak of the tension cycle, the numerically determined tension has a faster decrease rate than the measured one, for about half of the decrease leg.

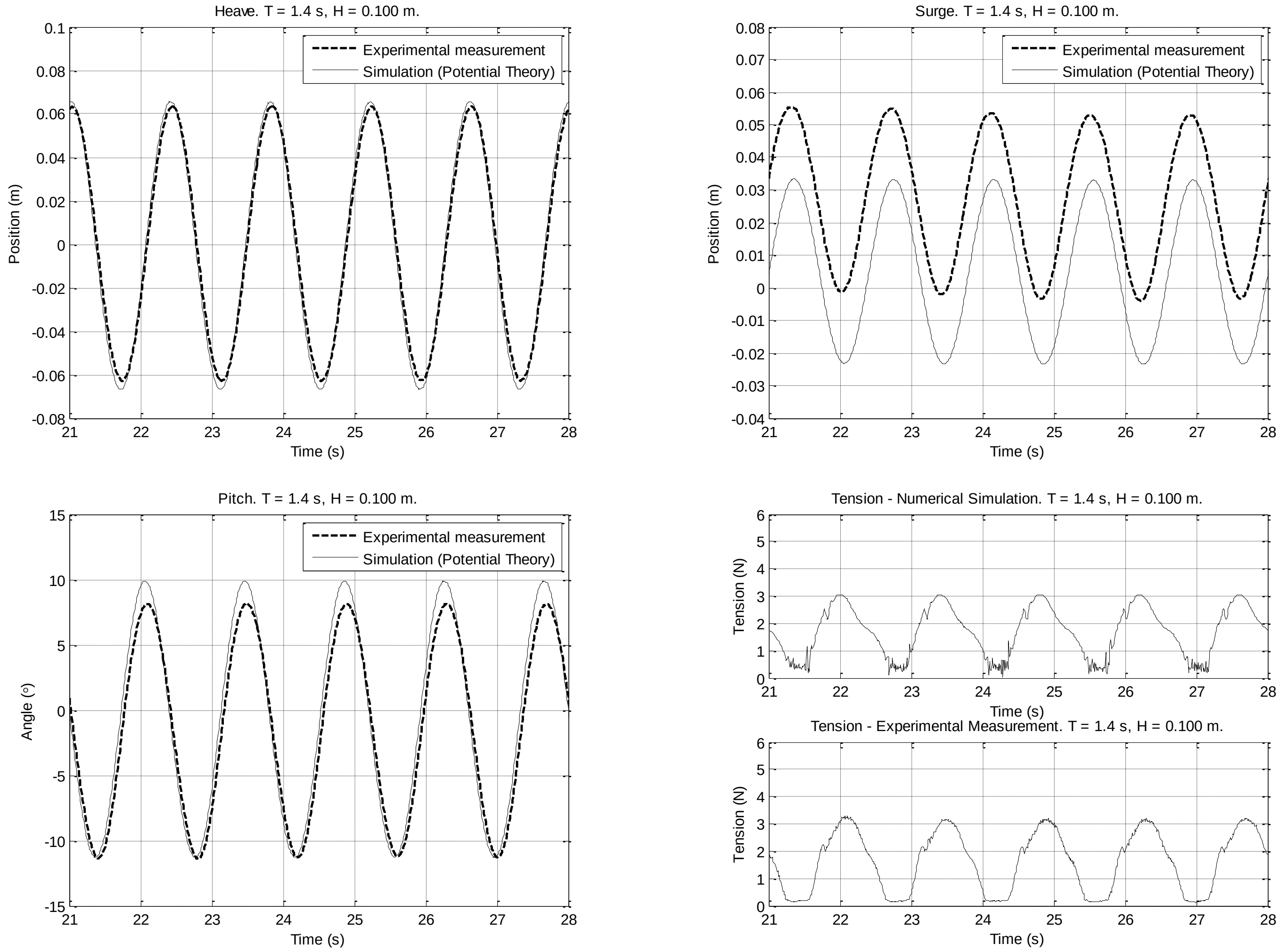

Figure 3. Results of the numerical simulations using linear potential theory. The motion plots are computed for the centre of floatation. Computed values for heave and pitch agree well with the measurements. In the surge motion, there is an offset in the measured mean position that is not reproduced in the simulations. As for the tension, although the numerical results are noisier than the measurements, the maximum value and the shape of the tension cycle are reasonably well captured.

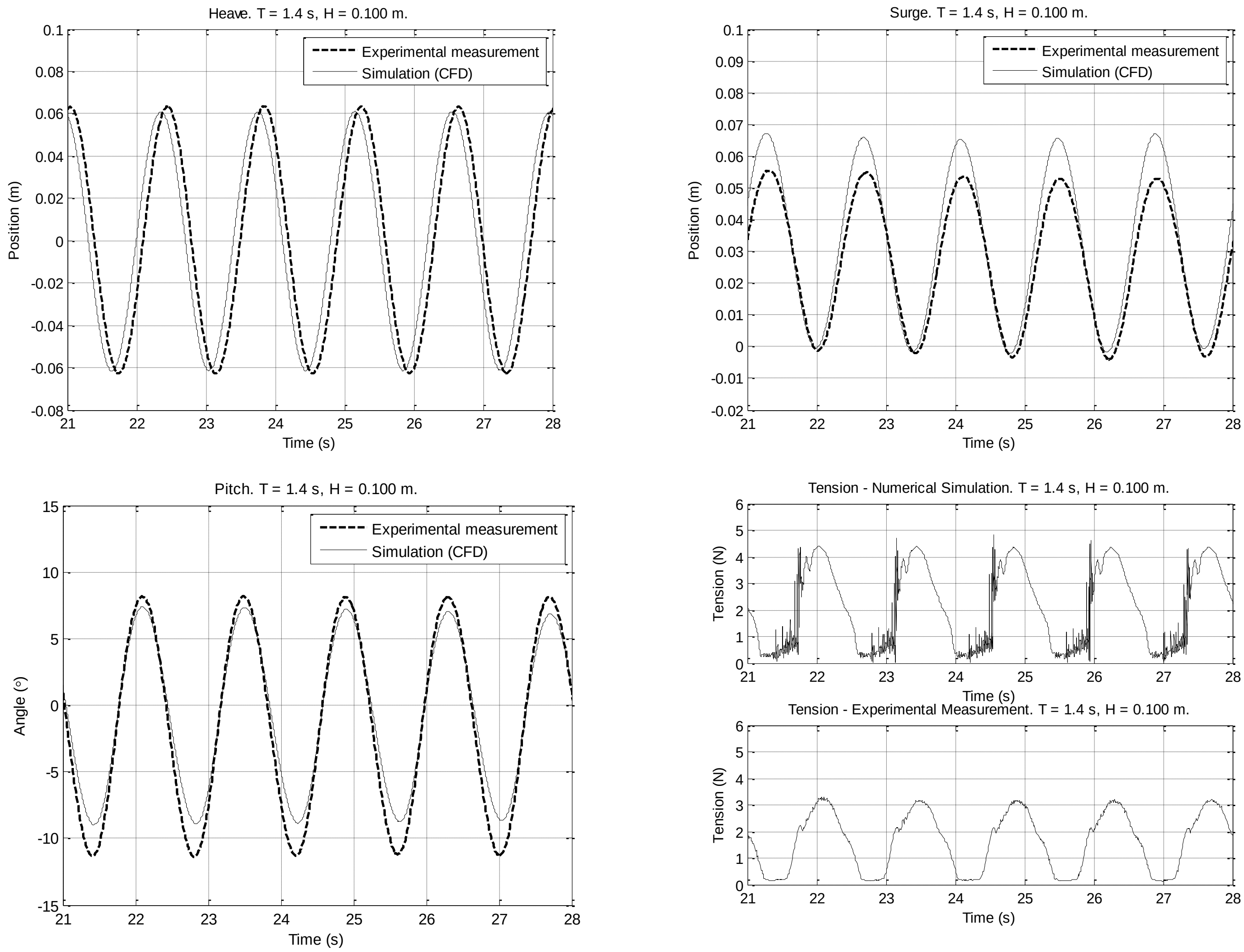

Figure 4. Results of the numerical simulations using CFD. The motion plots are computed for the centre of floatation. The computed motions agree well with the measurements, even though the phase offset is more significant. The surge motion is determined with greater accuracy than with linear potential theory. The tension force is computed without using filters, so the noise level is higher than in the simulation with potential theory. The computed tension has a higher amplitude than the measured tension, but there are uncertainties in the measured values.

4.2. CFD simulations

The results from the CFD simulations are presented in Figure 4.

The motion amplitudes are reasonably well determined. Heave and pitch havesmaller amplitudes than in the experiments, but surge has a larger amplitude. There are small phase offsets in all the motions.

The numerically determined tension is around 12 N higher than the measured one, but the shape of the cycle is well recreated.

Even though the mean surge position in the CFD simulations isn't the same as in the experiments (0.005 m larger), it is better determined than in the simulations using linear potential theory. The amplitude of the surge motion is around 0.01 m larger in the simulations than in the experiments.

The pitch amplitude is around 2 to 3 degrees smaller in the simulations than in the experiments.

When the tension is close to zero, the noise level is higher than in the simulations using linear potential theory and the noise increases sharply when the tension rises. There is also a spike just before the small indentation on the tension crest. In the CFD simulations, the exponential filters used in the simulations with linear potential theory weren't used. This is a numerical artifact that should not seriously affect the buoy frequency response, due to its highly transient behaviour.

5. Discussion

In the simulations using linear potential theory, the difference between the measured and the computed mean position of surge was caused by the second order wave drift forces that displaced the buoy from its mean position in the experiments.

These drift forces aren't modelled in the first order formulation of linear potential theory. As such, the second order drift isn't reproduced in the simulation and the residual drift in surge is caused by the surge damping and the pitch-surge coupling.

As an example of the effect of the drift forces, in Table 3 are presented the values of the measured surge drift, the horizontal force required to generate it and the resulting tension in the chain.

Table 3. The effects of second order drift forces. The drift forces displace the buoy relative to its mean position and increase the load sustained by the catenary, increasing its mean tension.

	REST POSITION	1.4 S WAVES
Measured Drift (m)	-	0.026
Horizontal force that causes the drift (N)	-	0.29
Static tension in the rest position (N)	1.77	2.06
Increase in Tension (N)	-	0.29

In the simulations using CFD, the surge is a bit larger than in the experiments, for reasons that are difficult to determine. There are differences in the incoming wave and there are also numerical fluctuations in the air phase, which can affect the surging motion and increase the mean drift force.

An important limitation affects the comparison of measured and simulated tensions: the load cell used in the experiments, even though submersible, was not pressure compensated. Because of this, in some parts of the load cycle, the tension in the cable may be up to 0.8 N higher than measured and the actual correction depends on the instantaneous position and orientation of the load cell and on the wave phase.

The tension force in the simulations using CFD is higher than in the simulations using linear potential theory, because the displacement induced by the drift forces increases the load on the cables in the CFD case. It is also higher than the measured tension in the experiments, around 1.2 N. Because of the limitations of the load cell used in the experiments, the actual tension in the cable may be up to 0.8 N higher than measured. This means that even though the estimated using CFD is larger than the measured one, it may, in fact, be closer to the real one. Part of the difference is also caused by the fact that the surge drift is overestimated.

When the tension is close to zero, the numerically determined tension is noisier than the experimentally measured one. This phenomenon has two causes: the singularity of the equation of motion of cables without bending stiffness at low tension (Burgess, 1992; Triantafyllou and Howell, 1994), and the nature of *hp*-finite LDG formulation itself. The effect can partly be compensated for through a careful application of filters.

There are small phase offsets between the numerically determined and experimentally measured motions. This can have numerous causes, such as a difference between the real and numerical values of the damping, of the added masses, of the excitation force phase, errors in the determination of the physical properties of the buoy (centre of gravity, inertia, etc), errors in the estimation of the position of the centre of floatation (which is the reference point for the rigid body motions), etc.

It was found that very small differences (around 0.005 m), in the measured position of the centre of gravity had some influence in the results, due to the change in the pitch stiffness and in the inertia around the centre of floatation. Even on a small scale model, such a high accuracy is not easily achieved due to the limitations of the technique used to determine these parameters.

6. Conclusions

Numerical simulations of a moored buoy were presented, where the mooring cable was modelled using the numerical model for cable dynamics MOODY and the buoy was modelled using two different methods: linear potential theory and computational fluid dynamics. These simulations were compared with experimental measurements.

The results showed that MOODY can be used to successfully model mooring cables, as the dynamics of the buoy and the tension in the cable are reasonably well captured. When using linear potential theory, the second order drift forces aren't accounted for and the surge drift isn't reproduced. This is overcome when CFD is used.

Limitations in the load cell used in the experiments cast some uncertainty in the measured tension values and, as a consequence, in the tension simulations.

The conditions tested are in the linear regime. Wave energy devices will also be subjected to storm conditions, where the effect of non-linearities may be significant. In this case, linear potential theory may not hold and CFD simulations may be required.

Acknowledgements

This work was funded by FCT – Fundacão para a Ciência e Tecnologia (the Portuguese Foundation for Science and Technology) through PhD grant SFRH/BD/62040/2009 and research project FCT-PTDC/EME-MFE/103524/2008b and by the Swedish collaboration platform Ocean Energy Centre (hosted by Chalmers University of Technology and supported by a grant from Region Västra Götaland, the regional development agency of Vöstra Götaland in Western Sweden).

References

Burgess, J. (1992). *Equations of Motions of a Submerged Cable with Bending Stiffness*. In CHAKRABARTI, S. K. et al. (Eds.) - Proceedings of the 11th International Conference on Offshore Mechanics and Artic Engineering. Calgary, Alberta, Canada : The American Society of Mechanical Engineers.

Chakrabarti, S. (1994). *Offshore Structure Modeling*. Singapore : World Scientific Publishing Co. ISBN 981-02-1513-4.

Cockburn, B.; Shu, C. W. (2001). *Discontinuous Galerkin Methods for Convection-Dominated Problems*. Journal of Scientific Computing. pp. 173-271. ISSN 0885-7474.

Jacobsen, N. Fuhram, D., Fredsøe, J. (2012). *A wave generation toolbox for the open-source CFD library: OpenFoam*. International Journal for Numerical Methods in Fluids. pp. 1073–1088. doi: 10.1002/fld.2726.

Johansson M. (1986). *Transient Motions of Large Floating Structures*. Göteborg. [s.n.].

Lindahl, J. (1985). *Modellförsök med en förankringskabel*. Göteborg. [s.n.].

Montano, A., Restelli, M., SACCO, R. (2007). *Numerical simulation of tethered buoy dynamics using mixed finite elements*. Computer Methods in Applied Mechanics and Engineering. pp. 41-44 doi: 10.1016.

Palm, J., Paredes, G., Eskilsson, C.; Taveira-Pinto, F., Bergdahl, L. (2013). *Simulation of Mooring Cable Dynamics Using a Discontinuous Galerkin Method.* In WRIGGERS, B. B.; P., R. (Eds.) - V International Conference on Computational Methods in Marine Engineering - MARINE 2013.

Palm, J., Eskilsson, C., Paredes, G., Bergdahl, L. (2013) - *CFD Simulation of a Moored Floating Wave Energy Converter*. In 10th European Wave and Tidal Energy Conference. Aalborg, Denmark. [s.n.].

Paredes, G., Eskilsson, C., Palm, J., Bergdahl, L., Leite, L., Taveira-Pinto, F. (2013) *Experimental and Numerical Modelling of a Moored, Generic Floating Wave Energy Converter.* In 10th European Wave and Tidal Energy Conference,. Aalborg, Denmark : [s.n.]

Triantafyllou, M., Howell, C. (1994). *Dynamic Response of Cables Under Negative Tension: an Ill-Posed Problem.* Journal of Sound and Vibration. pp. 433–447. ISSN 0022-460X. 173:4,